2012

Characterization of a CH planar laser-induced fluorescence imaging system using a kHz-rate multimode-pumped optical parametric oscillator

Joseph D. Miller
Iowa State University

Sascha R. Engel
Friedrich-Alexander-Universität Erlangen-Nürnberg

Johannes W. Tröger
Friedrich-Alexander-Universität Erlangen-Nürnberg

Terrence R. Meyer
Iowa State University, trm@iastate.edu

Thomas Seeger
Friedrich-Alexander-Universität Erlangen-Nürnberg

Characterization of a CH planar laser-induced fluorescence imaging system using a kHz-rate multimode-pumped optical parametric oscillator

Joseph D. Miller,[1] Sascha R. Engel,[2,3] Johannes W. Tröger,[2,4] Terrence R. Meyer,[1,2,*] Thomas Seeger,[2,4] and Alfred Leipertz[2,3]

[1]Department of Mechanical Engineering, Iowa State University, Ames, Iowa 50011, USA

[2]Erlangen Graduate School in Advanced Optical Technologies (SAOT), Friedrich-Alexander-Universität Erlangen-Nürnberg, 91052 Erlangen, Germany

[3]Lehrstuhl für Technische Thermodynamik, Friedrich-Alexander-Universität Erlangen-Nürnberg, 91052 Erlangen, Germany

[4]Lehrstuhl für Technische Thermodynamik, Universität Siegen, 57076 Siegen, Germany

*Corresponding author: trm@iastate.edu

Received 23 November 2011; revised 5 February 2012; accepted 6 February 2012; posted 6 February 2012 (Doc. ID 158799); published 8 May 2012

The performance characteristics of a new CH planar laser-induced fluorescence (PLIF) imaging system composed of a kHz-rate multimode-pumped optical parametric oscillator (OPO) and high-speed intensified CMOS camera are investigated in laminar and turbulent CH_4-H_2-air flames. A multi-channel Nd:YAG cluster that produces up to 225 mJ at 355 nm with multiple-pulse spacing of 100 μs (corresponding to 10 kHz) is used to pump an OPO to produce up to 6 mJ at 431 nm for direct excitation of the A-X (0, 0) band of the CH radical. Single-shot signal-to-noise ratios of 82∶1 and 7.5∶1 are recorded in laminar premixed flames relative to noise in the background and within the flame layer, respectively. The spatial resolution and image quality are sufficient to accurately measure the CH layer thickness of ~0.4 mm while imaging the detailed evolution of turbulent flame structures over a 20 mm span. Background interferences due to polycyclic-aromatic hydrocarbons and Rayleigh scattering are minimized and, along with signal linearity, allow semi-quantitative analysis of CH signals on a shot-to-shot basis. The effects of design features, such as cavity finesse and passive injection seeding, on conversion efficiency, stability, and linewidth of the OPO output are also discussed.

OCIS codes: 120.1740, 190.4970, 300.2530.

1. Introduction

The recent availability of high-repetition-rate, high-energy Nd:YAG lasers has led to an increased interest in high-speed planar laser techniques for understanding gas-phase combustion reactions in turbulent flows. The use of optical parametric oscillators (OPO) [1–3] and high-speed pumped dye lasers [4,5] is necessary for producing ultraviolet (UV) and near-UV tunable radiation for exciting electronic transitions in diatomic molecules. To investigate minor species (e.g., NO and CH) at repetition rates of 10 kHz and higher, the use of OPO instruments with high UV pulse energies (0.5–10 mJ) is of interest to avoid significant gain depletion, which makes high-speed-pumped dye lasers impractical [6]. Both custom-built [1,2,7–10] and commercially available

1559-128X/12/142589-12$15.00/0

OPO instruments [3] have been used to produce wavelength tunable UV radiation at repetition rates up to 1 MHz. The energy requirements have resulted in a series of high-energy pulse-burst lasers [11] and commercially available Nd:YAG clusters [3] to pump OPO instruments.

High-speed OPO instruments have been coupled with burst-mode and multi-channel (or clustered) Nd:YAG lasers to excite the OH radical [2,3], CH radical [8,10], and NO molecule [1,7,9]. Typically, the UV or near-UV tunable radiation is generated by mixing the OPO signal with the narrow-linewidth pump creating a UV-shifted pulse through sum-frequency mixing [2,7,8] or by frequency doubling the generated OPO signal [3]. In gaining the advantages of UV excitation, a corresponding reduction in pulse energy is incurred with multi-step conversion efficiencies of 0.5–1% of the pump energy [3,8]. While these pulse energies are low, in some low temperature cases or when stable molecules (NO) can be injected into an experimental system, they are sufficient for fluorescence imaging with high signal-to-noise ratio. This is not the case for species such as CH that naturally exist at parts-per-million (ppm) levels within the flame. To address the need for high pulse energies to excite the CH radical, the authors have recently reported a multimode-pumped broadband OPO which uses the signal to directly excite CH without frequency mixing or doubling [10]. Because the conversion efficiency to the signal reaches 10% or higher, pulse energies of up to 6 mJ per pulse are possible. While the broadband nature of the output is a disadvantage in terms of energy delivered to a particular rovibrational electronic transition, it also avoids saturation effects which are common with CH fluorescence [3,10,12,13].

The CH radical serves as an excellent marker of the high-temperature reaction zone in hydrocarbon combustion [13] and has been used to study dynamic fluid—flame interactions and flame stability [14–16]. Detection of the CH radical is difficult because it is a minor species in hydrocarbon combustion reactions and oxidizes rapidly. Until recently, single-shot measurements with high signal-to-noise ratio (SNR) were limited to one [12,13,16,17] or two pulses [14] at a 10 Hz repetition rate. Sets of ten CH PLIF images at 10 kHz have been collected with a peak SNR of 7:1 using a burst-mode laser [8], and the authors recently demonstrated 4 CH-PLIF images at 10 kHz with a peak SNR of 35:1 using direct excitation at 431 nm [10]. While most CH measurements have focused on excitation of the CH B-X (0, 0) transition at 390 nm and detection in the CH A-X (0, 0) band from 422–435 nm to eliminate interferences due to laser scatter, there are potential advantages in exciting CH at 431 nm for kHz-rate OPOs [10]. Generating 390 nm laser emission using the direct output of an OPO requires a 266 nm pump beam that is usually weaker, less stable, and less uniform than the 355 nm pump beam required for generating direct OPO output at 431 nm. Direct excitation at 431 nm also avoids interference from formaldehyde near 390 nm, which can be an important advantage for flame front imaging [18]. For open air combustors used for understanding turbulent fluid—flame interactions, surface scattering can be eliminated even for the case of resonance fluorescence, and Rayleigh scattering can potentially be used for shot-to-shot laser-sheet normalization or suppressed through high-pass filtering.

The goal of this work is to investigate the performance characteristics of a CH-PLIF imaging system that has been used for kHz-rate detection of the CH radical at 431 nm [10], and in particular the potential for quantitative measurements of CH signal intensity. Unlike the authors' work published in a recent Letter [10], this effort will examine signal-to-noise characteristics and flame structure in a laminar premixed flame similar to that used by other investigators [13]. This facilitates comparisons with current literature on CH-PLIF imaging. We will also extend the analysis to include signal-to-noise ratios between the CH layer and the background as well as within the CH layer itself. This, along with analysis of detector linearity and background corrections, will be used to evaluate the ability to measure CH layer thickness, observe turbulent flame structure, and quantify CH signal levels. In addition, the performance of the multimode-pumped OPO will be analyzed, including the effects of several design parameters such as cavity finesse and injection seeding on parameters such as conversion efficiency, spectral bandwidth, and corresponding shot-to-shot fluctuations. Such performance characteristics are important as the current laser architecture and imaging system have only recently been applied to high-speed CH-PLIF imaging.

2. Experimental Setup

A. High-Speed High-Energy Nd:YAG Cluster

The laser system in the current work is comprised of a custom-built OPO, pumped by a cluster of four double-pulsed, Q-switched Nd:YAG lasers at 1064 nm (Thales Multi-Channel Nd:YAG). Each laser can be double-pulsed with an inter-pulse spacing as low as 100 μs at maximum output energy, and independently controlled with spacing as low as 100 ns between adjacent lasers. Second-, third-, and fourth-harmonic generation crystals can be employed to generate individual pulses at 532 nm, 355 nm, and 266 nm respectively for all output pulses. In single pulse operation, the individual pulse energies are as high as 515 mJ at 532 nm, 225 mJ at 355 nm, and 130 mJ at 266 nm. In double-pulse operation the available energy is slightly reduced. For 355 nm operation, each line is individually converted to 355 nm and combined collinearly. The output energy is controlled using a waveplate—polarizer combination on the fundamental wavelength, therefore allowing equal pulse energy for each laser line. Although eight pulses are possible, only one was used in the current

work to characterize the performance of the PLIF system.

B. Optical Parametric Oscillator

The layout of the custom OPO is given in Fig. 1. It is composed of two β-Barium Borate (BBO) crystals which are rotated to provide walk-off compensation for the pump and signal wavelengths. The crystals (United Crystals, $7 \times 5 \times 15$ mm) are cut at 35 degrees in order to allow signal generation over a large range of wavelengths with both 355 nm and 266 nm pump sources, although only 355 nm is explored in the current work.

The BBO crystals are enclosed in a ring cavity composed of two high reflectors and one output coupler. The ring cavity design allows for directional pumping of the OPO with a signal that propagates in the clockwise (pump) direction. The high reflectors provide greater than 99% reflectivity from 375 nm to 460 nm, thus allowing the cavity to be used for a number of different signal generation schemes and producing a singly resonant oscillator on the signal. Two different output couplers with a nominal reflectivity of 40% and 60% from 390 nm to 460 nm were used in the current work. The variable reflectivity allowed the finesse of the cavity to be controlled to passively narrow the signal bandwidth.

The pump laser beam (3 mm diameter) interacts with the BBO crystals in the Type-I phase-matching configuration through two 355 nm mirrors with anti-reflection coating at the signal wavelength set into the ring cavity. After the first pass, the pump light is rerouted into the crystals a second time in a nearly identical propagation direction as the first pass. The second pass acts to both decrease the OPO threshold (~17 mJ) and increase the conversion efficiency at high pump energy (~9%) as described in our previous Letter [10].

An external cavity diode laser (ECDL) can be used to injection seed the OPO to further narrow the signal bandwidth. The 15 mW single-mode ECDL is wavelength tunable from 441–443 nm via a user-adjustable grating, and the injection seeding is performed on the signal wavelength (Sacher Lasertechnik, Littrow). Unlike previous work, which required a high-damage-threshold optical isolator [2], the seed beam is easily injected into the ring cavity through the output coupler due to the directional propagation of the generated signal. Although this configuration reduces the seed power in the cavity by the reflectance of the output coupler, 5 mW is sufficient for narrowing the signal bandwidth and the scheme dramatically reduces the chance of damaging the ECDL with only one low power isolator. In the current work, the pump laser is operated at 355 nm while signal is generated near 431 nm with a resulting idler of ~2000 nm, near the upper limit of BBO transmission.

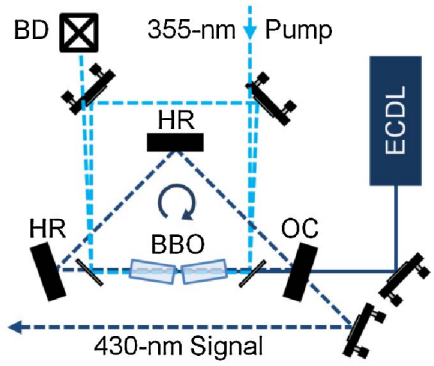

Fig. 1. (Color online) Schematic of the OPO showing double-pass configuration and seed source. OC: output coupler, HR: high reflector, BBO: β-Barium-Borate crystals, BD: beam dump, ECDL: external cavity diode laser.

The output signal was delivered to the test section using fused silica right-angle prisms, allowing the OPO to be tuned without the need for replacing the beam steering optics. The ~5 mm signal beam was expanded using a −50 mm UV cylindrical lens and collimated and focused using a +750 mm UV spherical lens. The low energy edges of the sheet were removed, producing a ~0.75 mm thick sheet with a nearly-collimated height of 65 mm. Although energies as high as 6 mJ per pulse for CH PLIF are achievable [10], working at lower pump energies enabled detailed characterization of OPO performance while avoiding potential damage to cavity mirrors and crystals. The laser energy was reduced even further to improve laser-sheet uniformity by removing low intensity regions, yielding an effective pulse energy of ~2 mJ.

In previous work [10], the OPO was pumped at 10 kHz, resulting in sufficient stability and energy for high-speed CH-PLIF imaging in a CH_4-H_2-air diffusion flame. Because the OPO uses solid-state BBO crystals for signal generation, the effects of photobleaching or thermal instability were either nonexistent or had no significant impact. In the current work, we show that careful alignment helps to ensure consistent performance for different output pulses of the Nd:YAG cluster, and we analyze the effects of OPO design parameters using single-shot mean and statistical quantities.

C. Premixed and Diffusion Flames

The CH-PLIF imaging system was characterized using a laminar premixed flame, and single-shot images were collected in a turbulent jet diffusion flame. The burner consisted of a fuel orifice with a diameter of 2 mm, surrounded by a cylindrical co-flow shroud of air with a hydraulic diameter of 48 mm. The laminar premixed flame was operated without co-flow air and flow rates of $CH_4 = 0.21$ standard liters per minute (SLPM), $H_2 = 0.32$ SLPM, and air = 1.92 SLPM. This yields an equivalence ratio of 1.45 and CH_4 fuel mixture fraction of 0.4, corresponding to the condition of maximum CH LIF signal reported by Sutton and Driscoll [13].

The turbulent diffusion flame was also operated with H_2 addition for the suppression of polycyclic aromatic hydrocarbons (PAH) [10,13]. The H_2 flow

rate was held constant at 1 SLPM and the CH_4 was varied from 9.6–12.6 SLPM (jet Reynolds numbers, Re_D, of ~5500 to 7000). The air co-flow was held constant at 22.5 SLPM. At the lowest Reynolds number condition, the turbulent flame was anchored to the burner surface, while at higher Reynolds numbers the flame became periodically lifted. The addition of H_2 had two primary effects: increasing the flame stability at higher Reynolds number by increasing flame speed and slightly increasing CH in the diffusion flame. These conditions are similar to those of Watson *et al.* who studied pure CH_4 diffusion flames [15] and were chosen to produce a range of turbulent features and flame stabilization locations for demonstration purposes.

The fuels were supplied by compressed gas cylinders and air was provided by a filtered constant pressure supply. Flow rates for the laminar premixed flame were controlled using a 0–0.23 SLPM rotameter for CH_4 (Analyt-MTC), a 0–0.57 SLPM rotameter for H_2 (Analyt-MTC), and a 0–2.5 SLPM rotameter for premixed air (Analyt-MTC). Flow rates for the turbulent diffusion flames were controlled using a 0–30 SLPM rotameter for CH_4 (Analyt-MTC), a 0–10 m^3/hr mass flow controller for H_2 (Bronkhorst), and a 0–50 m^3/hr mass flow controller for coflow air (Bronkhorst).

3. Results of Optical Parametric Oscillator Characterization

A. Effect of Output Coupler Reflectivity

As previously reported, the OPO threshold can be reduced and conversion efficiency increased by using multiple passes of the pump laser in the OPO cavity [10]. An unfortunate consequence of the multiple-pass pumping configuration is an increase in signal linewidth of ~20%. Although narrow linewidth is typically preferred for fluorescence spectroscopy, the increase in signal energy when utilizing the double pass pump configuration is significant. The performance of the custom-built OPO was investigated with both a 40% and 60% reflectivity output coupler. In simple terms, the cavity is singly resonant on the signal wavelength and acts as a low-finesse etalon which can be used to limit the linewidth of the signal output. The mean theoretical mode spacing, mode width, and finesse for the 40% and 60% output coupler cavities are given over the range of 420 nm to 460 nm in Table 1. The mode spacing is the same for both output couplers since the cavity length is unchanged, while the mode bandwidth is close to that measured in injection-seeded OPO instruments [1].

Table 1. Cavity Characteristics for Each Output Coupler from 420 nm to 460 nm

OC Reflectivity [%]	Mode Spacing [MHz]	Mode Width [MHz]	Finesse
41.2 ± 2	470 ± 10	140 ± 10	3.3 ± 0.2
57.4 ± 3.5	470 ± 10	80 ± 10	5.6 ± 0.6

For both output couplers, the variation in mode width and finesse are within ~10% of the mean value over the entire range.

To quantify the effect of the output coupler reflectivity on the OPO bandwidth, the average bandwidth of the OPO signal was measured as a function of both wavelength and output coupler reflectivity as shown in Fig. 2. Each data point is the average of 70 individually-fit spectra recorded using a 0.55 m spectrometer (Jobin Yvon SPEX, Triax Series 550) with an experimentally measured resolution of ~0.04 nm near 442 nm (2.4 cm^{-1}). To measure the bandwidth over a wide spectral range, the high reflectors were replaced by broadband metallic mirrors with a reflectivity >95%. To compare the results with the theoretical bandwidth of the crystals, the acceptance bandwidth of the BBO crystals was calculated using the SNLO Nonlinear Optics Code from Sandia National Laboratories [19] as shown in Fig. 2. The acceptance bandwidth represents the range over which the phase-matching process is sufficiently satisfied to exhibit parametric oscillation without adjusting the angle of the BBO crystals. Both of the OPO configurations produce bandwidths which are several times smaller than the acceptance bandwidth of the crystals. A reduction in bandwidth of 37% from 8.9 cm^{-1} to 5.6 cm^{-1} is observed between the 40% and 60% output couplers along with a 3× reduction in the average standard deviation of the measured bandwidth. This is similar to the 43% reduction in computed mode bandwidth from 140 MHz to 80 MHz as listed in Table 1. Additionally, no significant correlation between bandwidth and wavelength exists in the experimental data, although a significant trend is observed in the calculated acceptance bandwidth. This indicates that the OPO bandwidth is dependent on the finesse of the OPO cavity and can be passively narrowed by increasing the reflectivity of the output coupler to 60% with the added benefit of increasing the stability of the spectrally narrowed signal. It should be noted that no active narrowing is employed; thus the output does not attain the narrow bandwidth of an individual cavity mode which is much less than the experimental output of the OPO signal [20].

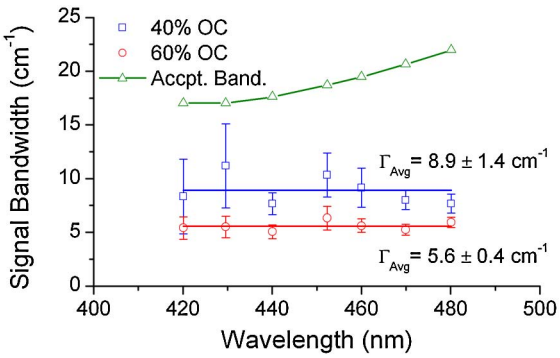

Fig. 2. (Color online) Bandwidth of OPO signal resulting from 40% and 60% output couplers (OC). Exponential function while the experimental data is shown with the computed average.

The impact of the output coupler reflectivity on both the linewidth and conversion efficiency of the OPO is significant. Although a desired decrease in signal bandwidth by ~40% is observed with the 60% output coupler, a decrease in output energy of 25% is measured. Higher finesse cavities, and thus narrower bandwidths, could be generated using higher reflectivity output couplers, but a reduction in output energy limits the practicality of this approach. Unlike injection seeding techniques, this reduction occurs because passive narrowing suppresses wavelengths outside the 5.6 cm^{-1} bandwidth determined by the output coupler reflectivity. In the current work, partial narrowing helps to maximize coupling with CH transitions in the Q-branch band-head region near 431 nm, but further narrowing must be balanced against the need for high output energy. Therefore, a technique for narrowing the signal bandwidth while maintaining or increasing the output energy is desirable.

B. Effect of Injection Seeding on Performance

Injection seeding has been shown to significantly increase the conversion efficiency of OPO devices along with reducing the operational threshold and providing stable, narrowed output [21]. This can be particularly advantageous in multimode pumped OPO devices where low signal energy and broadband output limit the spectroscopic applications of the systems. In many devices, injection seeding is performed at the idler wavelength which produces spectrally-narrowed signal following the conservation of energy, given that the pump laser is narrowed [1]. This can be advantageous since relatively-high-power diode lasers are limited in the visible and near-UV regions of the signal, and are more easily produced in the near IR region of the idler. In the case of a multimode pump source, as in the current work, injection seeding must be performed on the OPO signal since the conservation of energy can be satisfied to produce broadband signal using a broadband pump even if the idler is narrowed [22]. Unfortunately, diode laser sources are not common in the near-UV region, although some custom diode lasers are available near 431 nm. To evaluate the potential impact of injection seeding, however, an "in-stock" diode-laser at 442 nm was utilized here (Sacher Lasertechnik). Because 442 nm is not at the peak of CH absorption, results of this work could not be used to improve the performance of the CH-PLIF system. However, the data illustrate the feasibility of using injection seeding with a multimode pump source if an appropriate seed source can be manufactured. While this has been investigated with active cavity stabilization for low energy OPO devices, information on spectrally-narrowed multimode-pumped OPOs with high conversion efficiency and output energy of several mJ's is not available, yet important for spectroscopic applications in combustion.

A histogram of the measured signal bandwidth with and without injection seeding at 442 nm is shown in Fig. 3 for the double-pass configuration. For both conditions, the OPO is configured with the 40% output coupler to increase output energy. Additionally, no active cavity stabilization is employed in the current configuration in order to reduce complexity. A significant narrowing in bandwidth is observed as a result of injection seeding. Not only does the bandwidth decrease by ~2×, but the stability of the output also increases as is evident by the narrowing of the Gaussian fit to the data. The performance of the seeded cavity is similar to that observed by increasing the finesse of the cavity. A decrease in bandwidth of 46% from 8.2 cm^{-1} to 4.4 cm^{-1} is observed along with an increase in stability indicated by a decrease in standard deviation from 1.4 cm^{-1} to 0.6 cm^{-1}.

While injection seeding provides significant advantages, the bandwidth of the seeded OPO is still significantly larger than that expected from a cavity-stabilized injection-seeded multimode-pumped OPO [22] and is primarily due to a lack of active cavity locking. Highly effective injection seeding of a multimode pumped OPO requires a high finesse cavity to match a resonant mode of the cavity to the single-mode injection seed laser. When the frequency of the diode laser is closely matched to a resonant cavity mode, the OPO signal is limited by the characteristics of the cavity mode and diode laser. This typically requires a cavity yielding output energy on the order of 0.5 mJ. Recent work using 0.4 mJ of spectrally narrowed laser light has shown that only marginal CH fluorescence signal can be acquired under these conditions [8]. In contrast, the authors [10] and others [12] have previously shown that using high-energy, broadband signal can achieve nearly an order of magnitude increase in signal-to-noise ratio of the narrowband signal thus significantly increasing signal quality. In addition, a broadband source helps to avoid saturation by enabling excitation of multiple CH transitions. Therefore the use of injection seeding with no active cavity stabilization and the resulting 4.4 cm^{-1} broadband

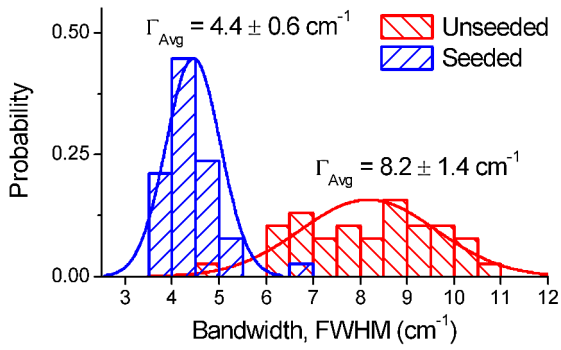

Fig. 3. (Color online) Effect of seeding on OPO spectral bandwidth and stability (as indicated by width of distribution). The experimentally measured resolution of the spectrometer is 2.4 cm^{-1}. Each data set is independent and full width at half maximum is determined using a Gaussian fit to the spectra.

output may be preferred over single-mode output with low laser energy.

If a seed laser is available at the appropriate wavelength, injection seeding would be advantageous over line-narrowing using cavity finesse. The experimental conversion efficiency of the OPO with and without injection seeding at 442 nm, is shown in Fig. 4 for the double-pass configuration with the 40% output coupler. In contrast to the 25% decrease in energy when the finesse of the cavity was increased, a significant increase in conversion efficiency is observed for the seeded output, reaching nearly 1.5× at 45 mJ pump. This increase is similar to that observed in injection seeded narrowband-pumped OPOs [1]. The advantages of injection seeding the passive OPO cavity are most easily observed by evaluating the energy per spectral unit. In this case, the output energy of the signal is increased by a factor of 1.6 while the bandwidth of the signal is reduced by a factor of nearly 2. This results in an effective increase of the energy per spectral unit (mJ/cm^{-1}) of nearly 3× over the unseeded signal. In contrast, increasing the output coupler reflectivity to increase the cavity finesse and decrease the signal bandwidth offers only a 1.4× increase. Thus the injection seeding method provides a twofold increase in energy per spectral element over the cavity finesse method and should result in an increased SNR. Even with a 2× increase in spectral energy density, the excitation should stay below the saturation limit for CH as reported elsewhere [13].

C. Multiple Pulse Performance

A significant advantage of the current instrument is the ability to operate the OPO at high-repetition rates without significant gain depletion, which is a limitation for high-speed-pumped dye lasers. In addition, the multimode pump source utilized in the current work is a commercially available, turn-key instrument. For demonstration purposes, the OPO was pumped with four pulses from the multi-channel Nd:YAG with a pulse separation of 100 μs corresponding to a repetition rate of 10 kHz. Because each line of the multi-channel laser must be individually aligned, the conversion efficiency of each line is highly dependent on the input vector in the plane of the phase matching angle. For a given crystal angle, each pump laser must be collinearly aligned to produce constant-wavelength signal with comparable energy. If the laser lines were overlapped carefully, then the conversion efficiency from pulse to pulse was fairly consistent, as shown in Table 2. Thermal effects, which might cause OPO performance to deteriorate for each subsequent pulse, were found to be negligible. Individual pump energies were monitored by tracking leakage through a pump mirror at 355 nm using a photo-diode-based energy meter (Thorlabs PM100D, ES111C). As the energy of this leakage was quite low, a 4 mm UG11 filter was used to eliminate residual 532 nm or 1064 nm laser light from the dichroic beam separators within the Nd:YAG cluster. The actual pump energy at the inlet to the OPO cavity was related to the photo-diode-based energy meter readings using an experimentally measured constant multiplier. In general, the pump energy of each laser line could be independently varied to allow for equal signal energy between pulses, typically within 10% of the mean. This is important since the detection system cannot be adjusted from pulse to pulse, and energy stability helps to avoid detector saturation and damage. One disadvantage of the current system is the large standard deviation in signal energy, reaching up to 50% at pump energies near the OPO threshold. As pump energy is increased the output energy becomes more uniform and the standard deviation is reduced significantly. As shown previously in Fig. 4, these fluctuations can also be reduced by injection seeding the OPO.

Table 2. Mean Pump and OPO Output at 431 nm Showing Consistent Conversion Efficiency for Spatially Overlapped Laser Lines #1–4

Laser	Pump [mJ]	Signal [mJ]	Conversion Efficiency [%]
1	45.57 ± 1.68	1.66 ± 0.56	3.64
2	37.84 ± 1.40	1.40 ± 0.41	3.70
3	39.91 ± 1.47	1.43 ± 0.73	3.58
4	43.74 ± 1.62	1.56 ± 0.31	3.70

The variation in spatial beam quality was investigated by measuring the profile of each laser line. The sheet was sectioned into 8 independent regions across the 65 mm sheet, and the energy was measured using a pyroelectric detector (Gentec Solo2, QE25SP). Each point was corrected for pump laser fluctuations and normalized to unity, as shown in Fig. 5. The system produces the best beam profile for laser line #4, which is expected since this laser path was used for initial alignment of the OPO and the other channels were aligned to be collinear to this path. Typically, only the middle 20–40 mm of each laser sheet was utilized to produce a nearly flat-top profile. The percent variation across the usable section of the sheet (10–50 mm in Fig. 5) was

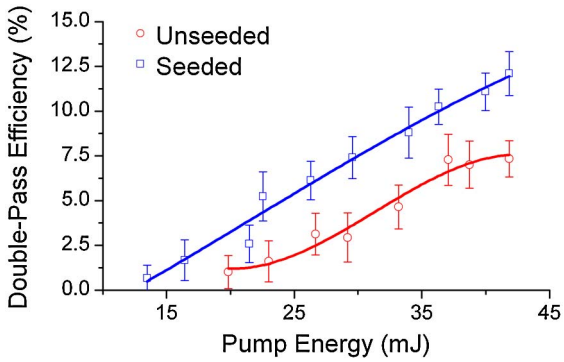

Fig. 4. (Color online) Effect of injection seeding on OPO performance for the double-pass pump configuration at 442 nm. Data are fit using a third-order polynomial.

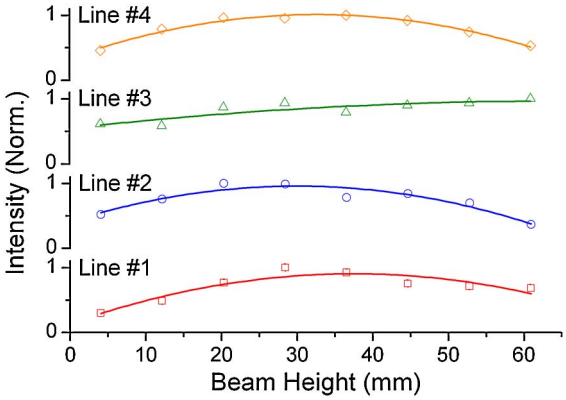

Fig. 5. (Color online) Average beam profile from 100 laser shots for pulses #1–4.

computed for lines 1–4 as 18.0%, 12.6%, 13.6%, and 10.4% respectively. The average beam profile for each line was used to correct average images for spatial variations. When possible, Rayleigh scatter from the cold air surrounding the flame was used to correct for shot-to-shot intensity variations.

4. Results of Detection Scheme Characterization

A. Spectral Discrimination

The fluorescence signal was collected using a high-speed camera (Photron SA5) coupled to a high-speed dual-stage intensifier (LaVision HS-IRO) and operated using DaVis software from LaVision. At 10 kHz, the camera resolution is limited to 768 × 768 pixels, and as many as four images were collected at 10 kHz [10], corresponding to the burst repetition rate of the multi-channel Nd:YAG laser. Light was coupled into the intensifier using a 50 mm visible Nikkor F/1.2 lens with two 8 mm lens extension rings to fill the intensifier with the region of interest. A relative gain (also referred to here simply as "gain") is selected in the intensifier software (0–100) which roughly corresponds to a linearized percentage of the maximum gain.

In our previous work, no filtering was employed in the CH PLIF imaging and detection system [10]. As a result, some interference from laser scatter was observed in the high-speed PLIF images. Separating the PLIF signal from scattering surfaces in the field of view using wavelength-shifted detection at ~435 mm (CH A-X (0, 0) P-branch) or ~489 mm (CH A-X (0, 1) band) present challenges [23]. At atmospheric pressure, electronic quenching can occur before significant redistribution of the population from the initial excited state and a thermal population distribution cannot be formed. This results in a fluorescence spectrum that is largely concentrated at the excitation wavelengths, with as much as 50% of the fluorescence residing in the initial levels for heterogeneous diatomic molecules such as CH and OH [23,24]. The CH A-X absorption profile was simulated in LIFBASE using the bandwidth of the signal as the instrument function and is shown in Fig. 6 [25]. In this work, the laser is tuned to the peak of the CH Q-branch absorption band at ~431 mm to maximize CH signal, although detectable signal is also achievable at lower excitation wavelengths near 429 nm. Both elastic Mie scattering from particles and surfaces and Rayleigh scattering from the gases are centered on the excitation wavelength at 431 nm. In this case, we have utilized a sharp-edged band-pass filter (Semrock FF01-445/20) with 99% transmission at 436 nm which falls to 50% at 432.5 nm and 1% at 429.9 as shown in Fig. 6. The upper limit (1% transmission) of the band-pass filter is 459.4 nm. This allows fluorescence from the P-branch to be detected in addition to 10% transmission from the initially excited levels near 431 nm.

While this filter does not completely eliminate laser scatter in this configuration, it does reduce the transmitted light at the excitation wavelength (431 nm) by over 10×. To evaluate the effectiveness of the filter at removing Rayleigh scatter, averaged CH PLIF images were acquired in a laminar CH_4–H_2-air premixed flame as described previously. The conditions were nearly identical to those of Sutton and Driscoll [13]. The average of 100 single-shot unfiltered CH-PLIF images with a gain of 60 is shown in Fig. 7(a), along with laser scatter from off-resonant excitation in Fig. 7(b), a PLIF image with off-resonant-subtracted scattering in Fig. 7(c), and a filtered CH-PLIF image in Fig. 7(d). The line plots are profiles across the flame layer 5 mm above the burner surface. Each CH PLIF image has been normalized to the maximum signal and corrected for the average laser sheet profile using Rayleigh scattering from the room-temperature air surrounding the flame. The flame profiles reveal signal in the center of the premixed flame for the unfiltered images (a, b) which is removed by subtraction of the off-resonant component and addition of the high-pass filter (c, d). This signal originates from Ralyeigh scattering from the cold fuel-air mixture and is related to the density of the gas. Although a detailed analysis of the Rayleigh scattering is outside the focus of this paper, we can observe that there is a jet of cool gases in the center of the flame as expected. This core is noticeably

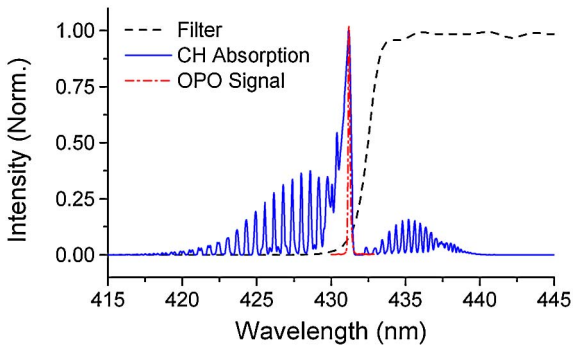

Fig. 6. (Color online) Overlap of filter transmission, CH absorption profile, and measured OPO signal. The CH absorption spectrum is simulated at 2000 K using LIFBASE with known resolution of the OPO signal.

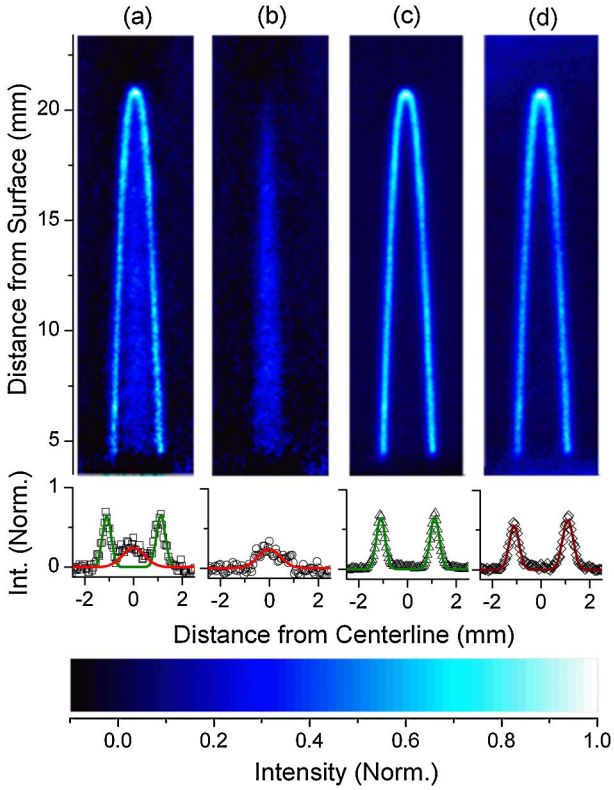

Fig. 7. (Color online) CH PLIF in a laminar premixed flame (false color). (a) Unfiltered image, (b) off-resonant unfiltered image, (c) unfiltered off-resonant-subtracted image ($c = a - b$), and (d) image with high-pass filter. The data are background subtracted, corrected to the beam profile using Rayleigh scatter in the vertical direction, and normalized to peak CH signal.

missing in the filtered images. Thus the inclusion of the high-pass filter effectively reduces the influence of Rayleigh scattering with respect to CH fluorescence using the current gain settings. Additionally, the off-resonant subtracted image (c) is nearly identical to the filtered image (d), as shown in the line profiles. Unfortunately, the filter reduces the interferences at the cost of decreasing the signal intensity. The filtered images exhibit significantly more noise along both the flame layer and in the background. Even so, the shape and relative intensity of the flame zone compares favorably with the unfiltered images.

B. Detector Response

The response of the signal intensity and noise is particularly important when using high-speed CMOS cameras and dual-stage intensifiers. Research on the use of these systems for quantitative imaging is relatively new [26,27], and little work has focused on spatial resolution and noise in thin flame layers. To determine the feasibility of semi-quantitatively correlating incident light to camera intensity, the response of the detection system to uniform incident light was investigated for gain settings similar to those used in the current work. A fiber-based white light source was used to illuminate the detector and a graduated neutral density step chart (Stouffer 21-Step Chart) was used to vary the light incident on the detector. Variations due to spatial inhomogeneity in the light source were corrected and the system response was determined. For all conditions the CMOS camera was background normalized prior to readout and an average background was subtracted to remove background interference. Up to 65% of saturation, the response is nearly linear while a third-order nonlinearity was observed above this limit. If a linear system response is erroneously applied to correlate camera intensity to light incident on the detector, the assumption results in an under-estimation of 20.7% at saturation. Hence, signals were kept below 80% of saturation not only to avoid damage to the intensifier, but also to ensure that the error associated with the linear response model is less than 10%. As noted in previous publications, even higher accuracies can be achieved by performing a detailed correction for detector noise, detector drift, and intensifier charge transfer for each pixel [26,27].

The system response was also investigated using CH-PLIF signals in the premixed flame. The signal for the flame layer and background are given as a function of relative intensifier gain in Fig. 8(a), while the background subtracted CH-PLIF signal is given as a function of excitation energy in Fig. 8(b) at a gain of 60. The CH-PLIF signal was quantified by averaging the signal along the CH flame layer from 5–20 mm above the burner surface. Because the CH layer is nearly uniform along the flame layer under these conditions, variations in the PLIF signal

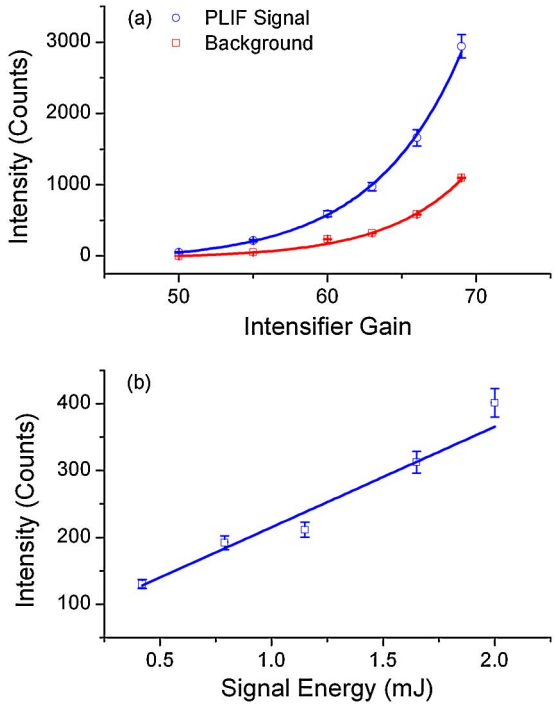

Fig. 8. (Color online) (a) PLIF and background signal as a function of relative intensifier gain with exponential fit and (b) linear response of PLIF signal to increase in excitation energy. Error bars represent the standard deviation among multiple measurements at the same experimental conditions.

represent the upper limit of random noise along the flame layer. We first observe that the measured CH-PLIF signal is an exponential function of intensifier gain. As gain is increased, the relative signal-to-background ratio decreases from ~5∶1 at a gain of 50 to a ratio of 2.7∶1 at a gain of 69, although the absolute intensity increases by 60× from 50 to 69. As discussed previously, the intensity should be kept below 80% of saturation (~3000 counts for the 12 bit monochrome camera) to maintain a nearly linear relationship between input light and detector counts. To maintain both high signal-to-background and absolute intensity, a gain of 60 was used to investigate the linearity of the CH PLIF signal, as shown in Fig. 8(b). A nearly linear relationship is observed between the excitation energy and the detected PLIF signal. Since we have verified that the detector response is also linear for the intensity and gain selected, this confirms that the CH PLIF is operating in the unsaturated regime. The use of unsaturated CH PLIF for quantitative signal analysis has several advantages over saturated LIF [28], although absolute calibration is beyond the scope of the current work. Even so, the current system shows the potential for such measurements.

C. Detector Noise

The ability to discriminate changes in PLIF intensity from detector noise is of particular significance and has not been previously studied for these high-speed intensified systems. Additionally, in previous CH PLIF work, the signal-to-noise ratio has been reported as the maximum signal to the noise of the background immediately surrounding the CH PLIF signal [8,10]. This definition highlights the ability of the system to detect thin CH PLIF layers from random background noise, which is very important in flame stability studies where CH is used as the primary marker of the reaction zone [14–17]. However, comparing the high CH signals in the flame layer to noise from the background signal, which is relatively low, does not represent the true SNR within the flame layer itself, which is a more relevant parameter for characterizing the ability to distinguish between regions of high and low CH signal. The SNR of the PLIF signal, defined here as the ratio of the maximum CH signal to the noise in the CH layer, is given as a function of relative intensifier gain in Fig. 9(a). The SNR of the PLIF-to-background SNR, defined here as the ratio of the maximum CH signal to the noise in the background, is given as a function of relative intensifier gain in Fig. 9(b). Both averages of 100 images and single-shot ratios are reported. The PLIF SNR in the flame layer is significantly lower than the PLIF-to-background SNR, which is the quantity typically reported in the literature [8,10]. Additionally, the single-shot SNR is lower than the SNR for average images for both PLIF signal and background. The PLIF SNR increases linearly with intensifier gain and the single-shot and average SNR in the flame exhibit nearly identical slopes. This

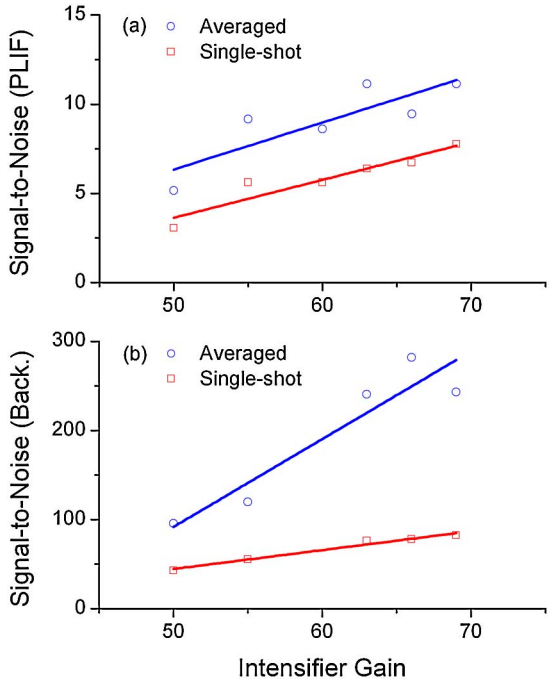

Fig. 9. (Color online) CH PLIF signal-to-noise ratio (a) within the flame layer and (b) relative to the background noise.

implies that the randomness of the noise in the flame layer is not a strong function of intensifier gain such that averaging of the images produces a similar reduction in noise at all gain levels. The PLIF SNR reaches 11∶1 and 7.75∶1 for the average and single-shot images, respectively, at a gain of 69. For the single-shot images, this is equal to 12.8% of the signal intensity. If we assume that we can discriminate a change in CH PLIF signal equal to twice the noise level, then we can quantify a minimum change in CH signal of 25% in a single-shot image at high speed.

The PLIF-to-background SNR is significantly better and reaches 300∶1 for the average image and 82∶1 for the single shot image at a gain of 69. The single-shot PLIF-to-background SNR is nearly the same as that reported using ~70 mJ from a broadband Alexandrite laser in a premixed flame

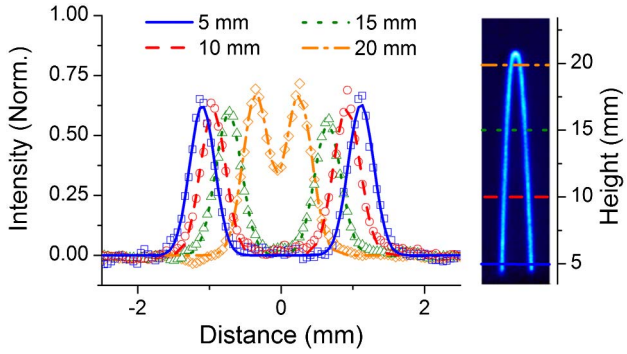

Fig. 10. (Color online) CH PLIF profiles across the premixed flame at 5 mm, 10 mm, 15 mm, and 20 mm above burner. Inset shows the height of each cross-sectional profile. Intensity is normalized to the maximum intensity in the flame layer.

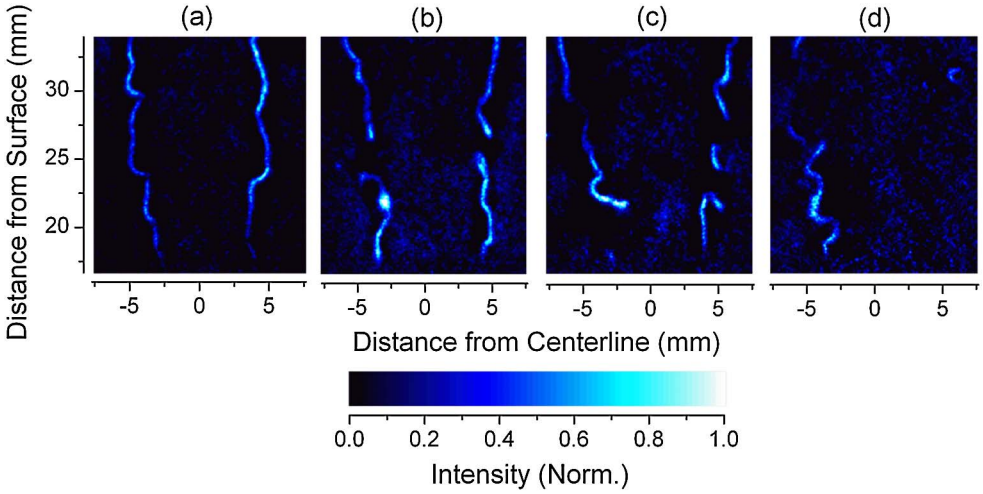

Fig. 11. (Color online) Single-shot CH-PLIF images in a turbulent diffusion flame with 1 SLPM H_2, 1.35 SLPM coflow air, and (a, b) 9.6 SLPM CH_4, (c) 11.8 SLPM CH_4, and (d) 12.6 SLPM CH_4. Each image is background subtracted, corrected for spatial beam profile variations using Rayleigh scattering, and normalized to the peak intensity of each frame.

[12]. It is also 3× the SNR we reported previously in turbulent diffusion flames [10]. While both the average and single-shot PLIF-to-background SNRs increase linearly with intensifier gain, the slope of the average SNR is much higher. This indicates that the randomness of the background noise is dependent on the gain such that the noise can be better filtered by averaging at high gain. Even with single-shot images, the ability to resolve the CH layer from the background is nearly equal to that previously reported using high-energy 10 Hz imaging systems.

D. Spatial Resolution

The addition of the intensifier also results in a reduction in the effective resolution of the detection system by shifting sensitivity to lower spatial frequencies. The ability to resolve thin layers is critical for studying the evolution and stability of flame layers using CH PLIF [15,16]. Patton *et al.* [26] identified small scale structures using Rayleigh scattering with a similar high-speed-detection instrument to a resolution of 100 μm verified using a pinhole. In previous CH PLIF work, flame layer thickness in premixed diffusion flames has been measured from 500–1200 μm, although the smaller scales may be underresolved as the result of saturation effects and the modulation transfer function of the detection system [29]. In the current work, the bimodal flame layer profile was fit using two Gaussian functions as shown in Fig. 10 and the full width at half-maximum (FWHM) of each layer was determined. The intensity and FWHM of each side of the flame layer are nearly identical, and the absorption which occurs in the left side of the flame is negligible. The flame layer has an average thickness of 426 μm with a minimum thickness of 410 μm at 5 mm above the burner surface. This compares favorably to previous measurements of flame layer thickness [29]. This FWHM is comprised of ~10 pixels giving a pixel resolution of ~50 μm.

5. Demonstration of Single-Shot CH PLIF Imaging

The CH PLIF imaging system was demonstrated in a turbulent diffusion flame as described previously. Both flame layer wrinkles and holes are clearly observed in the single-shot data in Fig. 11 where the Reynolds number increases from (a) to (d) by increasing the volumetric flow of CH_4. Fig. 11(a) and (b) are two independent frames from the same flame with Re = 5530. Most images display the continuous flame layers of (a), but intermittent holes open as shown in (b). As the Reynolds number is increased to 6670 in (c), the turbulent structures increase in intensity and more holes are observed. Additionally, the lower portion of the flame layer begins to lift as can be seen in the lower left corner. At a Reynolds number of 7090 in (d), the flame layer is highly wrinkled such that the right side of the flame layer is completely lifted and is, therefore, not present in the image. This is similar to the behavior observed in pure CH_4 diffusion flames by Watson *et al.* [16]. Both the flame layer structure and changes in the relative signal level are observable, including enhanced CH signals during vortex-flame interactions in images (a)–(d). The importance of maximizing SNR is illustrated in image (b), for example, where a signal drop of 75% in CH PLIF signal can be observed with lower signal levels still clearly distinguishable from the background noise.

6. Conclusions

A custom-built optical parametric oscillator (OPO) with signal at 431 nm and multi-mode kHz-rate pump source has been characterized for semi-quantitative CH planar laser-induced fluorescence imaging. The signal bandwidth is shown to depend on the OPO output coupler reflectivity, and therefore the cavity finesse, which also influences the conversion efficiency of the OPO. Additionally, the ability to frequency narrow the OPO signal via diode-laser-based injection seeding is demonstrated. Without

active cavity stabilization, a 2× reduction in bandwidth is observed along with a 1.5× increase in conversion efficiency. This yields a 3× improvement in spectral energy density over our previous work, although limitations on the availability of diode lasers make injection seeding impractical for CH PLIF at the current time.

Interference due to inelastic Mie and Rayleigh scattering is effectively minimized through the introduction of a band-pass filter and yields nearly identical results to that obtained with off-resonant background subtraction. The detector response is characterized and exhibits a nearly linear response to incident light, and the CH fluorescence is shown to be in the linear unsaturated regime. PLIF signal-to-noise ratios as high as 7.5 : 1 were measured in the single-shot images allowing variations of 25% to be quantified across flame layers, while single-shot PLIF-to-background signal-to-noise ratios up to 82 : 1 were measured. The latter is comparable to previous CH-PLIF measurements using low-speed sources. The detection system yields sufficient spatial resolution for resolving the thin flame layer thickness down to ~400 μm, which is comparable to previously measured values in similar flames. Finally, the ability to make single-shot measurements in turbulent diffusion flames is demonstrated. As Reynolds number is increased, the flame layers become more wrinkled and highly turbulent, developing large holes. At the highest Reynolds number the flame layer becomes highly destabilized as is evident in the experimental images. These performance characteristics indicate that the current high-speed source allows the shot-to-shot flame layer structure and variations in the CH signals to be tracked within the reaction zone of turbulent premixed and diffusion flames.

This work is supported by the Erlangen Graduate School in Advanced Optical Technologies (SAOT), funded by the German Research Foundation (DFG) in the framework of the German Excellence Initiative. J. Miller is supported through the National Science Foundation Graduate Fellowship Program. The authors are also grateful for ongoing discussions with W. Lempert (The Ohio State University), N. Jiang and S.Roy (Spectral Energies, LLC), M. Slipchenko (Purdue University), J. Gord (U.S. Air Force Research Laboratory), and P. Danehy (NASA).

References

1. N. Jiang, W. R. Lempert, G. L. Switzer, T. R. Meyer, and J. R. Gord, "Narrow-linewidth megahertz-repetition-rate optical parametric oscillator for high-speed flow and combustion diagnostics," Appl. Opt. **47**, 64–71 (2008).
2. J. D. Miller, M. N. Slipchenko, T. R. Meyer, N. Jiang, W. R. Lempert, and J. R. Gord, "Ultrahigh-frame-rate OH fluorescence imaging in turbulent flames using a burst-mode optical parametric oscillator," Opt. Lett. **34**, 1309–1311 (2009).
3. J. Sjoholm, E. Kristensson, M. Richter, M. Alden, G. Goritz, and K. Knebel, "Ultra-high-speed pumping of an optical parametric oscillator (OPO) for high-speed laser-induced fluorescence measurements," Meas. Sci. Technol. **20**, 025306 (2009).
4. I. Boxx, M. Stohr, C. Carter, and W. Meier, "Sustained multi-kHz flamefront and 3-component velocity-field measurements for the study of turbulent flames," Appl. Phys. B **95**, 23–29 (2009).
5. I. Boxx, M. Stohr, C. Carter, and W. Meier, "Temporally resolved planar measurements of transient phenomena in a partially pre-mixed swirl flame in a gas turbine model combustor," Combust. Flame **157**, 1510–1525 (2010).
6. C. F. Kaminski, J. Hult, and M. Alden, "High repetition rate planar laser induced fluorescence of OH in a turbulent non-premixed flame," Appl. Phys. B **68**, 757–760 (1999).
7. N. Jiang and W. R. Lempert, "Ultrahigh-frame-rate nitric oxide planar laser-induced fluorescence imaging," Opt. Lett. **33**, 2236–2238 (2008).
8. N. Jiang, R. A. Patton, W. R. Lempert, and J. A. Sutton, "Development of high-repetition rate CH PLIF imaging in turbulent nonpremixed flames," Proc. Combust. Inst. **33**, 767–774 (2011).
9. N. Jiang, M. C. Webster, W. R. Lempert, J. D. Miller, T. R. Meyer, C. B. Ivey, and P. M. Danehy, "MHz-rate nitric oxide planar laser-induced fluorescence imaging in a Mach 10 hypersonic wind tunnel," Appl. Opt. **50**, A20–A28 (2011).
10. J. D. Miller, S. R. Engel, T. R. Meyer, T. Seeger, and A. Leipertz, "High-speed CH planar laser-induced fluorescence imaging using a multimode-pumped optical parametric oscillator," Opt. Lett. **36**, 3927–3929 (2011).
11. N. Jiang, M. C. Webster, and W. R. Lempert, "Advances in generation of high-repetition-rate burst mode laser output," Appl. Optics **48**, B23–B31 (2009).
12. Z. S. Li, J. Kiefer, J. Zetterberg, M. Linvin, A. Leipertz, X. Bai, and M. Alden, "Development of improved PLIF CH detection using an Alexandrite laser for single-shot investigation of turbulent and lean flames," Proc. Combust. Inst. **31**, 727–735 (2007).
13. J. A. Sutton and J. F. Driscoll, "Optimization of CH fluorescence diagnostics in flames: Range of applicability and improvements with hydrogen addition," Appl. Opt. **42**, 2819–2828 (2003).
14. M. Tanahashi, S. Taka, M. Shimura, and T. Miyauchi, "CH double-pulsed PLIF measurement in turbulent premixed flame," Exp. Fluids **45**, 323–332 (2008).
15. K. A. Watson, K. M. Lyons, C. D. Carter, and J. M. Donbar, "Simultaneous two-shot CH planar laser-induced fluorescence and particle image velocimetry measurements in lifted CH_4/air diffusion flames," Proc. Combust. Inst. **29**, 1905–1912 (2002).
16. K. A. Watson, K. M. Lyons, J. M. Donbar, and C. D. Carter, "Simultaneous Rayleigh imaging and CH-PLIF measurements in a lifted jet diffusion flame," Combust. Flame **123**, 252–265 (2000).
17. Z. S. Li, B. Li, Z. W. Sun, X. S. Bai, and M. Alden, "Turbulence and combustion interaction: High resolution local flame front structure visualization using simultaneous single-shot PLIF imaging of CH, OH, and CH_2O in a piloted premixed jet flame," Combust. Flame **157**, 1087–1096 (2010).
18. J. Kiefer, F. Ossler, Z. S. Li, and M. Alden, "Spectral interferences from formaldehyde in CH PLIF flame front imaging with broadband B-X excitation," Combust. Flame **158**, 583–585 (2011).
19. SNLO nonlinear optics code available from A. V. Smith, AS-Photonics, Albuquerque, NM.
20. R. W. Boyd, *Nonlinear Optics* (Academic, 2003).
21. M. J. T. Milton, T. D. Gardiner, F. Molero, and J. Galech, "Injection-seeded optical parametric oscillator for range-resolved DIAL measurements of atmospheric methane," Opt. Commun. **142**, 153–160 (1997).
22. Y. B. He and B. J. Orr, "Tunable single-mode operation of a pulsed optical parametric oscillator pumped by a multimode laser," Appl. Opt. **40**, 4836–4848 (2001).
23. G. A. Raiche and J. B. Jeffries, "Laser-induced fluorescence temperature-measurements in a DC arcjet used for diamond deposition," Appl. Opt. **32**, 4629–4635 (1993).
24. K. J. Rensberger, J. B. Jeffries, R. A. Copeland, K. Kohsehoinghaus, M. L. Wise, and D. R. Crosley,

"Laser-induced fluorescence determination of temperatures in low-pressure flames," Appl. Opt. **28**, 3556–3566 (1989).
25. J. Luque and D. R. Crosley, "LIFBASE: Database and spectral simulation program (Version 1.5)," SRI International MP 99-009 (1999).
26. R. Patton, K. Gabet, N. Jiang, W. Lempert, and J. Sutton, "Multi-kHz mixture fraction imaging in turbulent jets using planar Rayleigh scattering," Appl. Phys. B doi:10.1007/s00340-011-4658-1 (2011).
27. V. Weber, J. Brübach, R. Gordon, and A. Dreizler, "Pixel-based characterisation of CMOS high-speed camera systems," Appl. Phys. B **103**, 421–433 (2011).
28. J. Luque and D. R. Crosley, "Absolute CH concentrations in low-pressure flames measured with laser-induced fluorescence," Appl. Phys. B **63**, 91–98 (1996).
29. C. D. Carter, J. M. Donbar, and J. F. Driscoll, "Simultaneous CH planar laser-induced fluorescence and particle imaging velocimetry in turbulent nonpremixed flames," Appl. Phys. B **66**, 129–132 (1998).